

CHAPTER II

RAPID DIAGNOSTICS FOR EBOLA GLYCOPROTEINS USING A QUARTZ CRYSTAL MICROBALANCE¹

Introduction

Ebola hemorrhagic fever (Ebola HF) is a deadly disease caused by ebolavirus that carries with it a 80% mortality rate in both infected human and non-human primates.² Because there is no cure, vaccine, or known reservoir for ebolavirus, outbreaks occur with little to no warning in regions with poor health care settings.² In response, researchers have worked on methods to detect ebolavirus using various techniques, such as reverse transcription polymerase chain reaction (RT-PCR),³⁻⁶ antigen capture enzyme-linked immunosorbent assay (ELISA),⁶⁻⁹ and reverse transcription-loop-mediated isothermal amplification (RT-LAMP).¹⁰ While these methods have shown some success, they lack the quick response time needed in a field transducer to help monitor outbreaks. For this reason, the quartz crystal microbalance (QCM) was developed as a rapid and sensitive method for the detection of ebolavirus glycoproteins (Ebola GPs) and killed whole ebolavirus, leading to eventual ebolavirus diagnostics.

Ebolavirus Antigen

Ebola (Figure 13) is a member of the family Filoviridae, and is classified as a select agent requiring biosafety level-4 (BSL-4) containment due to its high infectivity

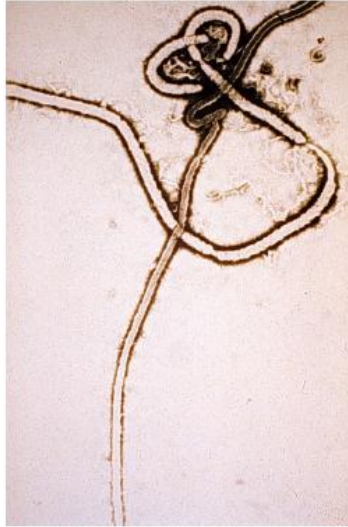


Figure 13. TEM image of ebolavirus.²

and lack of vaccine or treatment.¹⁰ Thus far, outbreaks of the virus have been isolated to regions of Africa, mostly the sub-Saharan areas.⁸ There are two genera in the Filoviridae, one being the Marburg virus, the other being the Ebolavirus and its four species: Zaire ebolavirus (ZEBOV), Sudan ebolavirus (SEBOV), Ivory Coast ebolavirus (ICEBOV), and Reston ebolavirus (REBOV).¹⁰ The last species (REBOV) has only shown infectivity in non-human primates and has not shown primate-to-human transmission. The four species of Ebolavirus are named for the regions from which they were first found, and each species has slight differences in structure.

Generally, ebolavirus is a negative-sense RNA virus containing seven viral structural proteins: nucleoprotein (NP), phosphoprotein (VP35), matrix protein (VP40), glycoprotein (GP), replication-transcription protein (VP30), matrix protein (VP24), and polymerase (L). There is an additional water soluble form of the GP called sGP or secretory GP.¹¹ Figure 14 is the structure shown by Sanchez and Rollin at the CDC for

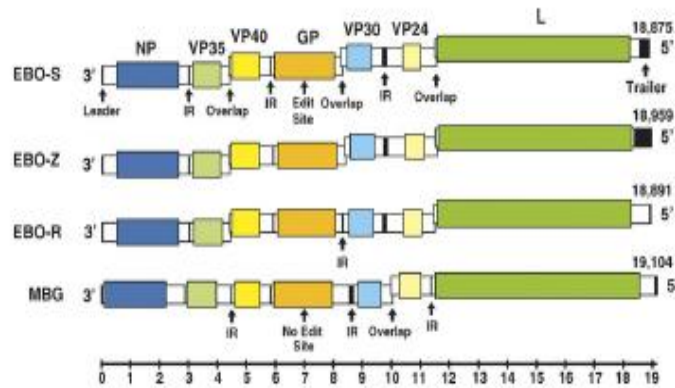


Figure 14. The seven viral structural proteins of various species of the Ebolavirus.¹¹

the seven viral structural proteins.¹¹ The average length for ebolavirus is reported as 19,000 nucleotides, but there is some variation from species to species and from genus to genus.

Work by Bavari's group and others has shown that ebolavirus actually stops dendritic cells from maturing to create an immune response.^{6,12} They showed this behavior with both live and inactivated virus, demonstrating that any antigen with all seven viral proteins will cause cells to shut down. The main finding of the work is that a virus like particle (VLP) with only the GP and VP40 matrix protein (both responsible for assembly of the virus) can allow the dendritic cells to mature and create an immune response to the virus. These VLPs lack the genetic material needed for replication, but

do mimic the assembled virus because of the role these two proteins play in self-assembly.

Previous work has shown the ability to detect some of the viral proteins from ebolavirus. The nucleoprotein has been detected using RT-PCR and ELISA techniques, and has been known to show some discrimination among strains.^{4,5,7,9} While successful, these techniques are still labor intensive, and require in depth training to carry out the procedure. Both techniques have the advantage of being field portable and capable of on-site testing. Time is another major factor for all the tests, as well. Generally, the ELISAs are coated overnight and used the next day, and the RT-PCR tests require at least two hours of gel amplification and multiple steps to complete detection. The strength of QCM is that it can be rapid (<20 minutes) and is very sensitive to the nanogram scale.

This chapter focuses on detection of the glycoprotein from ebolavirus, specifically from the Zaire and Sudan-Gulu strains. The glycoprotein is a thought to be the only superficial protein on the virus and is believed to aid in cell entry.¹² It is also one of the proteins responsible for immune responses, although it is not clear if it works in tandem or as the primary protein. This does, however, make the GP an ideal target for antibodies because they could neutralize the virus if they prevent cell entry.

Using already developed antibodies to the GP, we will build a QCM biosensor to detect the GP. QCM can be used to measure mass adsorption on a surface in a rapid, sensitive manner. The mass adsorption can be as simple as metal vapor deposition, and as complex as antibody-antigen binding or thin film layers. However, in order to effectively measure and quantitate the binding system, the principles and relationships behind QCM must first be described.

Mass Calculations via QCM

QCM uses AT-cut quartz crystals with gold electrodes in contact with an oscillating voltage to create a resonator. The crystal is driven to resonance frequency by the property of the converse piezoelectric effect, which states if an electric field is applied, a mechanical strain is created.¹³ If the instrument oscillates the electric field, then the piezoelectric quartz will undergo oscillating mechanical strains. QCM

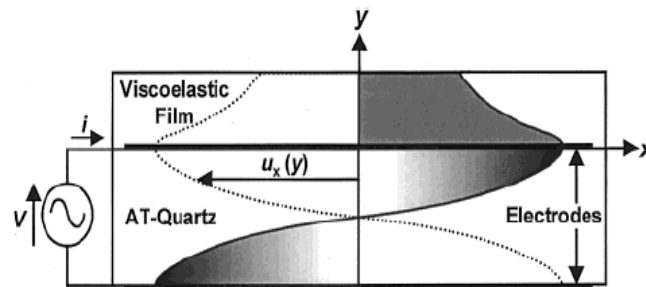


Figure 15. Oscillation of a Thickness Shear Mode (TSM) crystal.¹⁴

operates using a voltage supply that oscillates at a given frequency in contact with the gold electrodes deposited on the quartz. This generates the electric field to create the mechanical stress across the crystal face. Figure 15 shows how a wave generated via mechanical deformation propagates out of the crystals into the viscoelastic film.¹⁴ The measured decay of the wave from a 5 MHz crystal is ~250 nm in water.¹³ The decay length limits how extended the layers can be from the surface before the instrument loses sensitivity.

Saurbrey first developed QCM in 1959 with his discovery of a linear relationship between the frequency changes of a piezoelectric crystal with the addition of mass to the surface (Eq. 1),¹⁵

$$\Delta f = -C_f \Delta m \quad (\text{Eq. 1})$$

Δf is defined as the change in frequency, C_f is a sensitivity factor, and Δm is change in mass on the oscillating crystal. This assumes a rigid, tightly coupled layer on the surface.^{13,16} The C_f factor can be further expanded to account for various attributes of the quartz resonator that are constant, with the exception being the frequency. When C_f is expanded it provides the more comprehensive evaluation in (Eq. 2),¹⁷

$$\Delta f = -2\Delta m N f_o^2 / [A(\mu_q \rho_q)^{1/2}] \quad (\text{Eq. 2})$$

In this equation N is the overtone number, μ_q is the shear modulus of quartz (2.947×10^{11} g/(cm*s²)), and ρ_q is the density of the quartz (2.648 g/cm³). The term $\Delta m/A$ is the density, which is dependent on the layer fabrication and any deformations. The one factor that is commonly manipulated is the f_o , or frequency of the unperturbed crystal. Inherent to (Eq. 2) is that increasing f_o will increase the sensitivity factor by the square of the value, whereby the same mass addition will give boosted signal (Δf) for a higher frequency crystal. This also means that the C_f varies based on f_o . The constant for 5 MHz crystals is experimentally known to be 0.0566 Hz/ng/cm², and for a 9 MHz resonator the value increases to 0.1834 Hz/ng/cm², both determined at 20 °C.¹⁸

While this approximation worked well for initial gas phase metal deposition and other open air experiments, it did not hold true when QCM began to be used in liquid systems. Liquid based methodologies are extremely necessary when biosensors are applied to native biological conditions, since most biologicals are buffered or at the very

least purely aqueous. Liquid loading would cause viscoelastic effects arising from the solvent and could cause overestimations of mass loading.^{13,17,19} To account for the loading effects of density and viscosity from the contact liquid Eq. 1 is modified as seen below (Eq. 3),

$$\Delta f \sim -C_f \Delta m - C_f (\Delta \rho \eta / 4\pi f_o)^{1/2} \quad (\text{Eq. 3})$$

The second term is related to the liquid loading effect, but it is not discernable from the mass loading in this equation. In order to discriminate mass loading due solely to adsorption, the liquid effect must be de-coupled from this equation, which gives rise to a second much needed measurement, R_L .

R_L is the resistive liquid loading, and only depends on density and viscosity (Eq. 4),¹⁶ which are the terms that need to be corrected for in a liquid based QCM measurement.

$$\Delta R_L \sim (\eta_q / [c_{66} C_1]) + (N\pi C_1)^{-1} (\Delta \rho \eta / \pi f_s c_{66} p_q)^{1/2} \quad (\text{Eq. 4})$$

From this equation, η_q is the effective quartz viscosity, c_{66} is the quartz elastic constant,

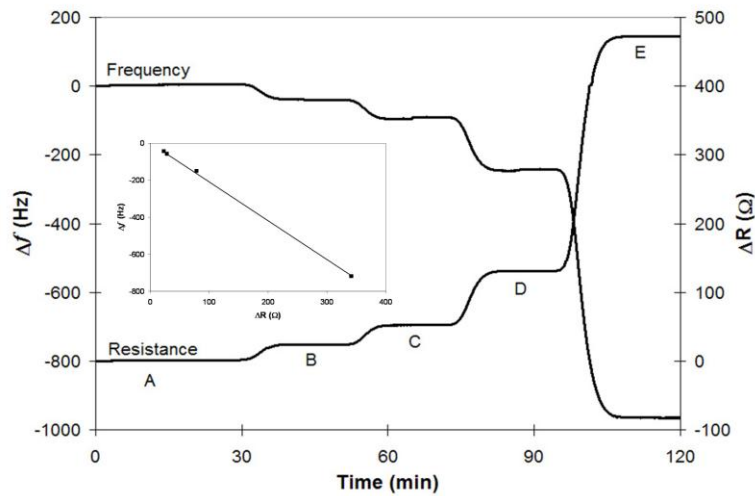


Figure 16. Frequency and resistance changes measured while increasing the concentration of a sucrose solution. Inset linear plot gives the slope for the correction factor.

C_1 is the motional capacitance of the unperturbed crystal, N is again the overtone, and ρ_q is still the quartz mass density. While the instrument measures R_L , a calibration is needed to know the magnitude of correction from the term. To do the correction, a solution that does not interact with the surface (varying concentrations of glucose and sucrose are commonly used) is flowed over the sensor, and causes frequency and resistive changes, Figure 16. Since, the changes are not from actual mass loading; one can calculate a correction factor for pure resistive loading, essentially the slope of the Δf vs. the ΔR .

Then by re-arranging Eq. 1, the mass of the system can begin to be solved for (Eq. 5),

$$\Delta m = -\Delta f / C_f \quad (\text{Eq. 5})$$

By taking in to account the sensitive area and the resistance measurement with correction, the equation is then expanded to form the final calculation. The end mass equation is then (Eq. 6 and 7), for a 5MHz and 9MHz, respectively. The C_f factors are adjusted for the sensitive area ($A = 34.14 \text{ mm}^2$) of the crystal by dividing C_f by A to give 165.54 Hz/ug and 536.41 Hz/ug.

$$\Delta m = (-\Delta f + (2.095 * \Delta R)) / 165.54 \quad (\text{Eq. 6})$$

$$\Delta m = (-\Delta f + (2.095 * \Delta R)) / 536.41 \quad (\text{Eq. 7})$$

Binding Kinetics

While absolute mass measurements are a necessity, QCM can elucidate additional information about a binding system. One such benefit from QCM's real time measurement is the ability to derive binding constants and kinetic data. Binding

constants will quantify how strongly an antibody recognizes an antigen, and will allow a direct method of comparison between different pairs. To accomplish these goals, a Langmuir isotherm is used as a model to determine binding constants.

The Langmuir isotherm works well for most surface binding systems with some constraints. The three main assumptions are that there is only monolayer coverage, all surface sites are equivalent, and adsorption to one site is independent of the condition of the adjacent sites.²⁰⁻²³ The first point is easy to assume, while the second assumption relies on the quality of the surface, which can contain a variety of defects. However, the defects can be minimized through polishing the crystal, and it has been shown that the energy differences from defects are small enough to ignore for the Langmuir.²² Under ideal conditions the third assumption holds true as well, however, systems with multivalent attachment to larger antigens are still possible.

For simplicity, the antibody-antigen system can be described as a monovalent receptor (antibody, Ab) interacting with a monovalent ligand (antigen, Ag).²¹ The system would form a complex as seen here: $Ag + Ab \leftrightarrow Ag-Ab$. This can be described in terms of an equilibrium expression (Eq. 8),

$$K_a = [Ag-Ab] / ([Ab])([Ag]) \quad (\text{Eq. 8})$$

where K_a represents the equilibrium association constant. If the receptor is rigidly attached to a surface, one can look at the system in terms of an adsorption isotherm. The isotherm will relate the amount of adsorbed analyte, the concentration of analyte in solution, and K_a .

In order to find K_a , one first looks at the fractional coverage (θ), which relates to the percentage of the monolayer formed, given by (Eq. 9),²¹

$$\theta/(1-\theta) = K_a C \quad (\text{Eq. 9})$$

C is defined as the concentration of the bulk solution. By increasing concentration, or by using a system with a higher K_a , we can increase the total surface coverage. From the QCM standpoint of measuring mass, the amount of antibody determines the maximum amount of antigen that can be bound. Therefore, the change in mass from the antigen (Δm) is related to the fractional coverage and the immobilized surface (antibody) is related to the maximum change in mass (Δm_m). K_a can be determined with these factors and a means of comparison between couples is now possible. These new assignments transform the fractional equation into the isotherm (Eq. 10),

$$\Delta m = \Delta m_m [K_a C / (1 + K_a C)] \quad (\text{Eq. 10})$$

This equation, when plotted, shows an increase in adsorption versus concentration, but the plot follows a non-linear shape. To obtain a linear fit, a reciprocal plot can be made by rearranging (Eq. 10) to (Eq. 11),

$$\Delta m = -(K_a)^{-1} (\Delta m / C) + \Delta m_m \quad (\text{Eq. 11})$$

In using (Eq. 11), the plot is made using Δm and $\Delta m / C$, and K_a is found as the inverse of the slope. Also, Δm_m can be determined from the y-intercept.

Because QCM is done in real-time, kinetic information can be derived to supplement the association constant.^{21,23-26} Both the forward and reverse rate constants, k_f and k_r (or k_a and k_d), are found by looking at the surface coverage at specific time points. The initial equation states the change in degree of surface coverage (θ) with time, based on the forward and reverse rates in (Eq. 12),^{21,23,25}

$$k_a(1-\theta) = k_d\theta \quad (\text{Eq. 12})$$

If (Eq. 12) is integrated using a LaPlace Transformation, it can be rearranged to (Eq. 13), assuming $\theta(t) = 1$ at $t = \infty$ and $C = \infty$.

$$\theta(t) = [C/(C + K_a^{-1})] (1 - \exp[-(k_f C + k_r)t]) \quad (\text{Eq. 13})$$

If one makes $(C + K_a^{-1})$ equal to θ_∞ , and makes $k_f C + k_r$ equal to the time constant (τ^{-1}) , then (Eq. 13) simplifies down to (Eq. 14),

$$\theta(t) = \theta_\infty [1 - \exp(-\tau^{-1} t)] \quad (\text{Eq. 14})$$

The QCM mass measurements can be related to the surface coverage variables seen in (Eq. 14). This is because the mass measured and the θ are both based on concentration, so fractional coverage $\theta(t)$ can be related to $\Delta m_t / \Delta m_m$ at a given time and θ_∞ is assumed to equal 1, which substitutes to give (Eq. 15),

$$\Delta m_t = \Delta m_m [1 - \exp(-\tau^{-1} t)] \quad (\text{Eq. 15})$$

The mass variables can be pulled from information obtained in (Eq. 11). In the plot of $\ln[1 - m_t/m_m] = -t/\tau$, the logarithm is plotted versus time, and the slope is $-1/\tau$. With the new time constant and the known experimental concentrations, another plot is made of $1/\tau$ vs. C , where the slope of the line is equal to k_f and the y-intercept is equal to k_r .²³ Because $K_a = k_f/k_r$, the ratio of the kinetic rates can be use for comparison with the isothermal methods. Regardless of the route, these numeric measurements provide a solid means to compare the binding strength of antibody-antigen pairs.

QCM Applications in Biosensing

The principles and calculations described above have been applied by numerous groups to create QCM biosensors. Table 1 summarizes QCM biosensors of note from the

Virus	Sample Matrix	Target Antigen	Accuracy for Real Samples	Limit of Detection (LOD)	Standard Deviation (RSD)	Comparison on Method
Influenza ²⁷	PBS	HA Peptides on MPCs	Not available	2.3 nM	12% (n=6)	none
Dengue Fever ²⁸	Human Sera and PBS	Dengue Virus	80% (5 pos./ 10 neg)	0.7 µg/mL	26%	PCR ELISA
SARS Corona Virus ²⁹	Aerosolized sputum	Inactivated SARS-CoV	Not reported	0.6 mg/mL	14% (n=10)	Reusable 13x, over 60 days
Hepatitis B ³⁰	PBS	Viral DNA probe	Not reported	0.02-0.14 µg/ml	12% (n=7)	Reusable 5 times
Hepatitis C ³¹	Human Sera and PBS	Viral RNA	Not reported	Not Reported	25%	Amplicor Assay (PCR)
HIV ³²	Human Sera and PBS	HIV Antibodies of gp41	100% (4 pos./ 7 controls)	Not reported	Not reported	ELISA Western Blot
Herpes 6 Strains ³³	PBS	Herpes virus (6 strains)	Not reported	5 x 10 ³ virus particles	1.3% (n=10)	none
M13 Phage Inovirus ³⁴	PBS	Whole Phage	Not reported	5(10 ⁶) PFU/ml	±39% (n=9)	none
Bovine Ephemeral ³⁵	Bovine Sera and PBS	Whole Virus	Not reported	5 µg/mL	13.9%	ELISA
African Swine Fever ³⁶	Swine Sera and PBS	Virus Protein p12/ Virus Protein 73	Not reported	1 µg/mL	Not reported	none

Table 1. A detailed summary of selected antigens detected using QCM as the biosensor. All QCM samples were finished in less than 10 minutes, while the fastest comparative method, ELISA, was 2 hrs. or more. PFU = Plaque forming units, HA = Hemagglutinin, PBS = Phosphate buffered saline.

literature. Both the matrix and analyte show the versatility associated with using QCM. The immunosensor can operate in a matrix as simple as blood and as complex as human sera and sputum. Also, it can detect a range of analytes including the whole virus, phage, or smaller peptides and proteins.

The utilities of the QCM arise from the ability to functionalize the gold crystal surface in a myriad of ways. Because of well known gold-thiol chemistry, self assembled monolayers (SAMs) can be built from varying length alkanes with different functional head groups³⁷⁻⁴⁴ or from peptides.^{45,46} These SAMs can, for example, then be used to attach antibodies covalently to the surface. By varying alkane chain length, there is a high degree of control over the surface height and the freedom of movement for attached species on the sensor head. More freedom allows for the antibodies on the SAMs to find their proper confirmation with an antigen, but at the same time, the QCM will not tolerate films that are too lossy or viscous. Different head groups allow for more diversity in attachment strategies, whether by electrostatic charge interactions,^{42,47} by different reaction paths to form covalent bonds between groups, EDC/NHS coupling⁴⁸ or dithiol formation,⁴⁹ for example. Peptide monolayers can also be used to bind antibodies by specifically recognizing a sequence on the antibody and therefore, binding it to the sensor.

Another route for antibody immobilization involves the use of capture agents targeted at the antibodies.^{16,29,50-54} Specifically, Protein A, G, and L are commonly employed to bind antibodies via different recognition interactions. Protein A and G bind antibodies by their Fc region, which leaves the Fab region open for binding to their antigen. Protein L actually uses the kappa light chains near the Fab ends to bind the

antibody.⁵⁰ The proteins themselves are held on to the gold by a hydrophobic pocket that nonspecifically binds to the hydrophobic gold surface. Protein A has four strong binding sites ($K_a = 10^8$ /mole) and protein G contains two such sites.⁵⁵ Since Protein A and G have slightly different affinities for Fc, based on the antibodies subclass and species of origin, they can be tailored to fit the biosensor's requirements.

Experimental

Materials

Ebola GPs, monoclonal antibodies (15H10, 6D11, 17A3), and polyclonal antibodies were all graciously donated from the Southeast Regional Center of Excellence for Emerging Infections and Biodefense (SERCEB), specifically by Dr. Barton Haynes of Duke University, and stored at $-80\text{ }^\circ\text{C}$ until used. Phosphate buffer saline (50mM phosphate, 150 mM saline at pH ~ 7.2) was made from solid NaH_2PO_4 (Fisher) and solid NaCl (Fisher). Water-soluble Sulfosuccinimidyl 4-(N-maleimidomethyl) cyclohexane-1-carboxylate (Sulfo-SMCC), Dithiothreitol (DTT), and water-soluble *bis*[sulfosuccinimidyl] suberate (BS^3) were purchased from Pierce Biotechnologies. Aminoethanethiol (AET) and Sephadex G-10 were purchased from Sigma-Aldrich. Water was supplied from a $\sim 18\text{ M}\Omega$ NanoPure Diamond (Barnstead) with UV source for sterilization. Protein A, G, and L were purchased from Pierce Biotechnologies. Research Quartz Crystal Microbalance, 5MHz Ti/Au, and 9MHz Ti/Au were purchased from Maxtek, Inc. A four channel pump system and microbore santoprene tubing (1/16 I.D.) were purchased from Masterflex[®]. ACS grade 30% H_2O_2 and ACS grade concentrated

sulfuric acid were purchased from Fisher. Acetate buffer was made as 0.2 M at pH ~4.5 from acetic acid and sodium acetate, both from Fisher.

Crystal Cleaning

Crystals were cleaned using standard procedures.¹⁸ Briefly, a mixture of concentrated H₂SO₄ :30% H₂O₂ was mixed in a 3:1 ratio. While the solution was still hot, it was applied dropwise onto the crystal surface, left for one minute, washed with DI water and ethanol, and blown dry with nitrogen. The procedure was repeated four times, or more as needed.

Stock sample preparation

Stocks of protein A and G were made by dissolving the lyophilized solid (5 mg) in 1 mL PBS. Then, solutions of 500 µL protein A or G were made at a concentration of 4.5 µM in a 50/50 mix of PBS/acetate buffer. Antibodies were diluted from stocks to 500 µL aliquots at a concentration of 133 nM (20 µg/mL, MW = 150 kDa) in PBS. BSA solid was dissolved in PBS to a final concentration of 1 mg/mL. Antigen was used in various concentrations: 14 nM, 64 nM, 96 nM, 128 nM, and 192 nM all in PBS.

Antibody-Capture Agent Biosensor Fabrication

QCM crystals were placed in the Maxtek flow cell with the large electrode facing the air, and the semi-circle electrodes making contact on the POGO[®] pins. The flow cell holder was then tightened and the buffer was flowed at 30 µL/min. The fabrication of this style (capture agent-antibody) biosensor (Figure 17) has been performed extensively

in the literature.⁵⁶ Initially, the buffer was flowed for 30 minutes to an hour until a constant baseline was obtained. Next, 500 μL of the capture agent (Protein A/G/L) was flowed at a concentration of 4.5 μM for 10 minutes. Then, the buffer was passed again for 10 minutes to restore a new baseline after the mass addition of the Protein A/G/L. Buffer was followed by 500 μL of BSA run at 1 mg/mL to block the remaining gold

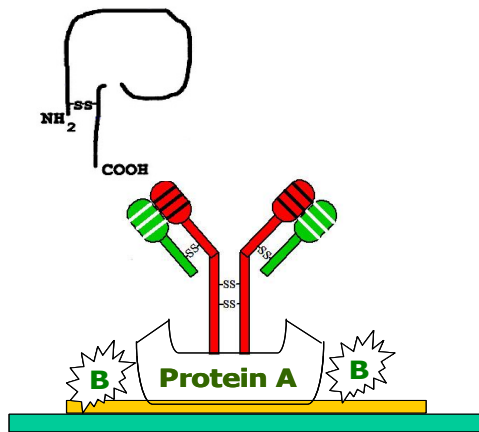


Figure 17. Representation of the biosensor, showing the Protein A base, BSA blocking (B's), and antibody orientation.

surface from any non-specific binding. After another 10 minutes of buffer, 500 μL of antibody was flowed at a concentration of 133 nM (20 $\mu\text{g/mL}$) and binding to the capture agent was observed. After antibody, 10 minutes of buffer was flowed to removed unbound antibody and re-establish a baseline. The last step was to present the antigen at various concentrations (14-196 nM) to observe binding to the antibody. Buffer was flowed after antigen to remove non-specifically bound antigen and establish a final baseline. After all the mass addition, the Δm were used to calculate rate constants and equilibrium binding constant.

Data Filtering

QCM data was filtered using LabView 7, setup as a low pass filter. The program was written and tested by Dr. Rachel Snider. Data was entered as a text file into a pre-programmed screen, including only the final calculated mass. Filtering was then carried out by testing multiple frequency values to obtain the optimal fit. Data was filtered to remove repetitive noise from pumps and sample changes, but not enough to add false features (the smoothing or creating of peaks). Any filtered data was displayed with the frequency value (Hz) used for that particular run.

Results and Discussion

Antibody Capture Assays¹

The first step in ebola GP detection relied on capturing ebola GP specific monoclonal and polyclonal antibodies on a capture surface made of Protein A, G, or L. The most successful biosensor utilized a combination of Protein A capturing mAb 15H10, followed by the detection of the GP. The combination's success was due mostly likely the result of two factors. The first is the high affinity of Protein A to 15H10 based on its subclass (IgG2a), which created a biosensor with a higher density antibody layer. The second was that 15H10 was determined to have a better affinity to both GP strains, slightly more so to Zaire. Figure 18 shows the progression of the mass loading with Protein A, BSA, mAb 15H10, and lastly the GP. The Protein A had a surface bound mass of $1.8 \pm 0.2 \mu\text{g}$. BSA commonly showed little to no mass binding, which is excellent in biosensor formation because our capture agent is covering more of the

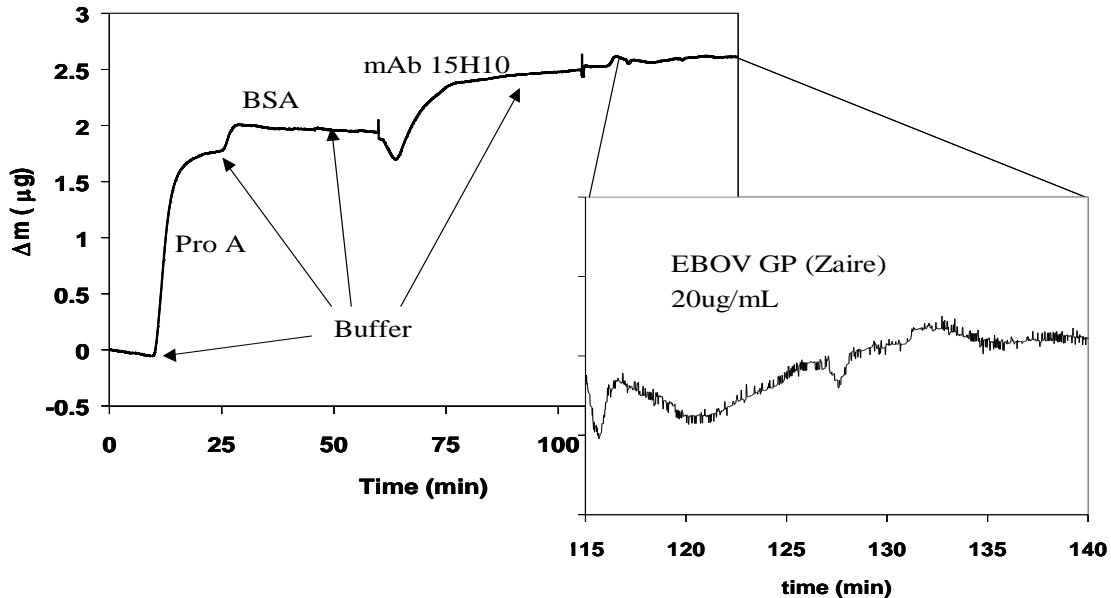


Figure 18. Mass loading curves for the detection of the Zaire GP. The blown up graph shows the successful binding of a 20 $\mu\text{g/mL}$ sample.

surface. The small mass change between Protein A and BSA is from a buffer switch (50:50 acetate:PBS to PBS), however, no mass is actually added during that time. The mAb 15H10 shows $0.6 \pm 0.1 \mu\text{g}$ of antibody binding onto the Protein A. After binding, the 15H10 did not begin to wash off, showing the sensor is stable for a long period of time, and the antibody off rate is very, very small. The GP was then run last, tested at multiple concentrations; Figure 18 shows a 20 $\mu\text{g/mL}$ (133 nM) sample run of the Zaire GP, which shows 60 ng of binding.

The mAb 15H10-GP combination had a limit of detection (LOD) of 10.5 ng, based on the S/N calculated at 3σ . By running a variety of concentrations, we were able to deduce the concentration limits based on the S/N. Figure 19 shows the various masses detected at different concentration. The horizontal line is the detection limit from the 3σ

calculation. The Zaire GP (solid line) and Sudan-Gulu (dashed line) have concentration LODs of 14nM and 56nM, respectively. From all 4 combinations attempted, the 15H10-Zaire GP pair showed the best promise for continued work due to its low LOD. Kinetic and equilibrium constants were calculated for the mAb 15H10-GP pair. Figure 20 shows each run that was performed for the Zaire and Sudan-Gulu strains, with change in mass plotted vs. concentration. They follow typical Langmuirian behavior in that, as concentration of bulk solution is increased, an increase in bound mass is also observed, until at a high enough concentration, the biosensor saturates. The Zaire GP gave a K_a of $9 \pm 1 \times 10^6 \text{ M}^{-1}$. To check this calculation, the forward and reverse rate constants were determined (k_f and k_r), which give values of $8 \pm 1 \times 10^3 \text{ M}^{-1}\text{s}^{-1}$ and $1.9 \times 10^{-3} \text{ s}^{-1}$. By analyzing the ratio of k_f/k_r , a K_a of $4.1 \times 10^6 \text{ M}^{-1}$ was calculated and which was found to be in good agreement with the isotherm association constant.

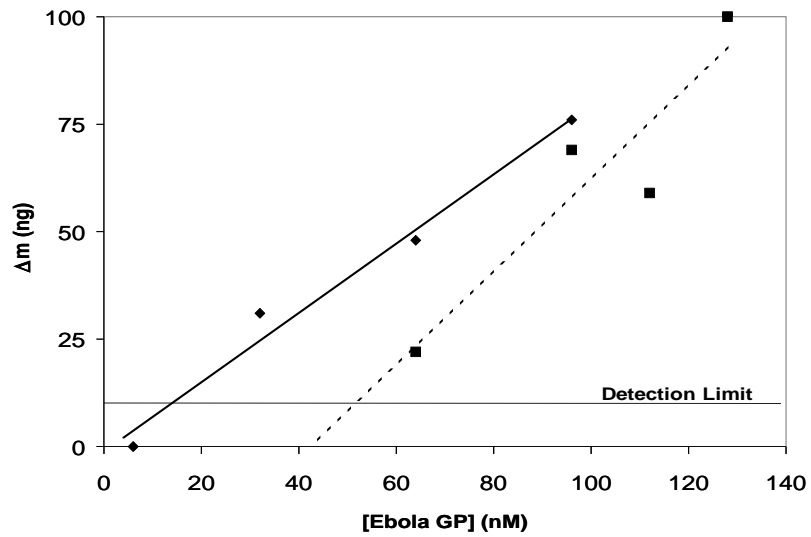


Figure 19. Concentration plots from the Zaire (solid) and Sudan-Gulu (dashed) GP. The detection limit is determined from the systems noise.

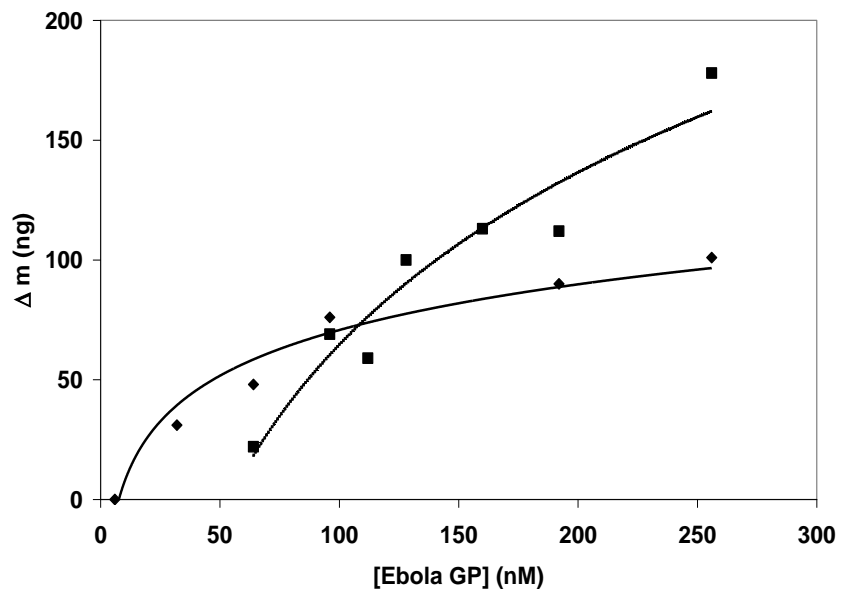


Figure 20. Langmuir plot of the Zaire GP (diamonds) and Sudan-Gulu GP (squares). The Zaire strain shows good curve fitting at saturation.

The second most successful mAb that was used to detect the GP was IgG1 6D11.

In order to immobilize this antibody, Protein G was used as the capture agent. From

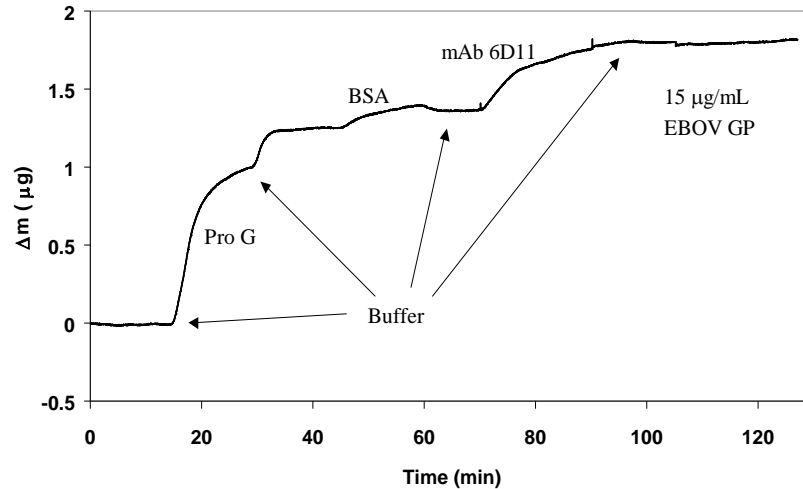


Figure 21. Gravimetry of mAb 6D11 used with Protein G.

Figure 21, one can see the mass loading of Protein G ($0.9 \pm 0.2 \mu\text{g}$), which tended to be less than that of Protein A. This is most likely due to less multi-layer formations or the smaller mass of Protein G. After Protein G, the same acetate/PBS to PBS rise is seen; again this is solely due to buffer switching and not additional mass gain. The blocking agent, BSA, is then added and minimal binding is observed, usually in the $0.2 \mu\text{g}$ range. BSA binding was then followed with antibody loading. Our average mass for antibody loading was $0.56 \pm .09 \mu\text{g}$, which is very consistent with the data obtained for 15H10, meaning the surface coverage was similar in both cases. However, when it came to GP binding, 6D11 did not recognize the antigen as well as 15H10, almost by a power of ten. The LOD in this case was 130 nM for Zaire and 160 nM for Sudan-Gulu, using a 3σ of 11 ng. The change in mass versus concentration is shown in Figure 22, and the fit does

not follow a Langmuir pattern. The Zaire GP had the closest fit to a Langmuir isotherm, but still has a very large error when trying to fit it for K_a or kinetic constants. The Sudan-

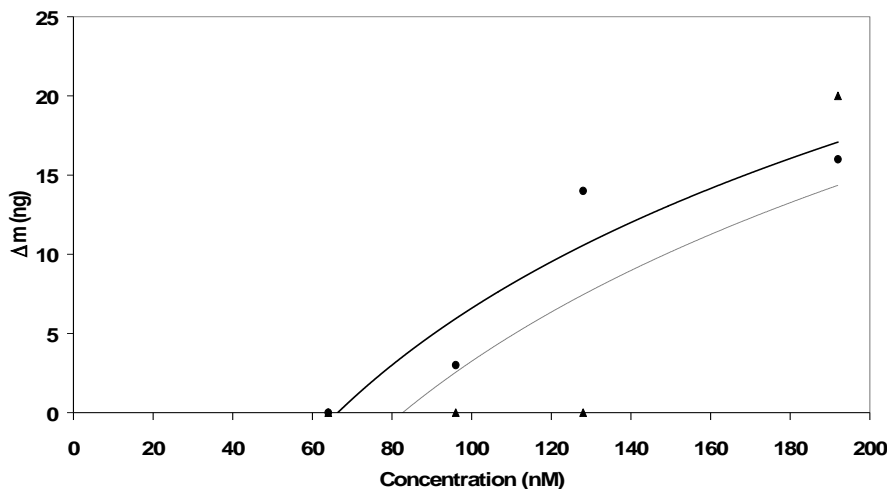


Figure 22. Langmuir plot of the 6D11 trials. The Zaire GP is shown as circles, while the Sudan-Gulu GP is the triangles. Both show large errors in the fitting.

Gulu follows a non-specific binding curve, where low concentrations show no mass loading, and high concentrations show dramatic increases in binding.

The last mAb used to detect Ebola GP was the IgM 17A3. Since this antibody was not part of the IgG subclass, a capture agent that uses Fc region recognition would not work. The 17A3 was an IgM which has a pentamers shape with all the Fc regions buried internally. Seen in Figure 23, Protein L was selected because it binds through kappa light chains that are located in the Fab region. Because of the pentamer shape, some of the Fab regions can be attached to Protein L while other regions remain available to binding antigens in solution. From the mass binding curve, Protein L does not show as much adsorption onto the gold layer, multiple experiments only showed binding of $0.36 \pm$

0.04 μg . This is unusual as Protein L is approximately the same molecular weight as Protein G and A, and was diluted in solution to the same isoelectric point. It is possible that Protein L does not have the same hydrophobic pockets as Protein G and A, therefore

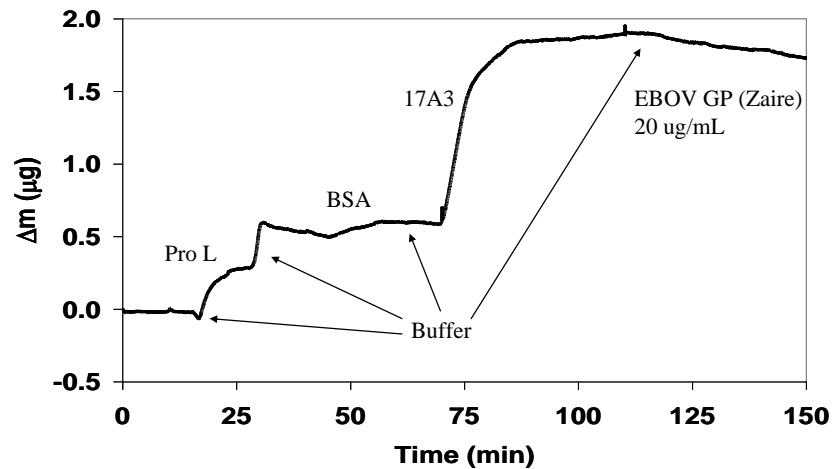


Figure 23. Resulting gravimetric loading using mAb 17A3. In the final step, no GP is seen binding to the surface.

causing a weaker attachment. 17A3 bound very well, experiments showed $1.3 \pm 0.1 \mu\text{g}$ of binding on average. This higher binding total could be attributed to the larger mass of the IgM. Using this antibody, no binding to the GP was ever observed, even at concentrations above 196 nM (30 $\mu\text{g}/\text{mL}$). Because this level of GP showed recognition in the other mAbs, experiments did not exceed this concentration. It should be noted that further experiments by the collaborators at Duke, who developed the antibodies, actually showed the 17A3 lacked any specificity to the GP, which validates the conclusions about non-specific binding.

The last sample tested for GP detection was the polyclonal serum from the rabbit immunization of the ebola peptides from the C-terminal peptide of the GP, Figure 24. Protein A was again used for these experiments because the antibodies were known to be IgG. The polyclonal binding step showed a very large mass gain compared to the mAbs,

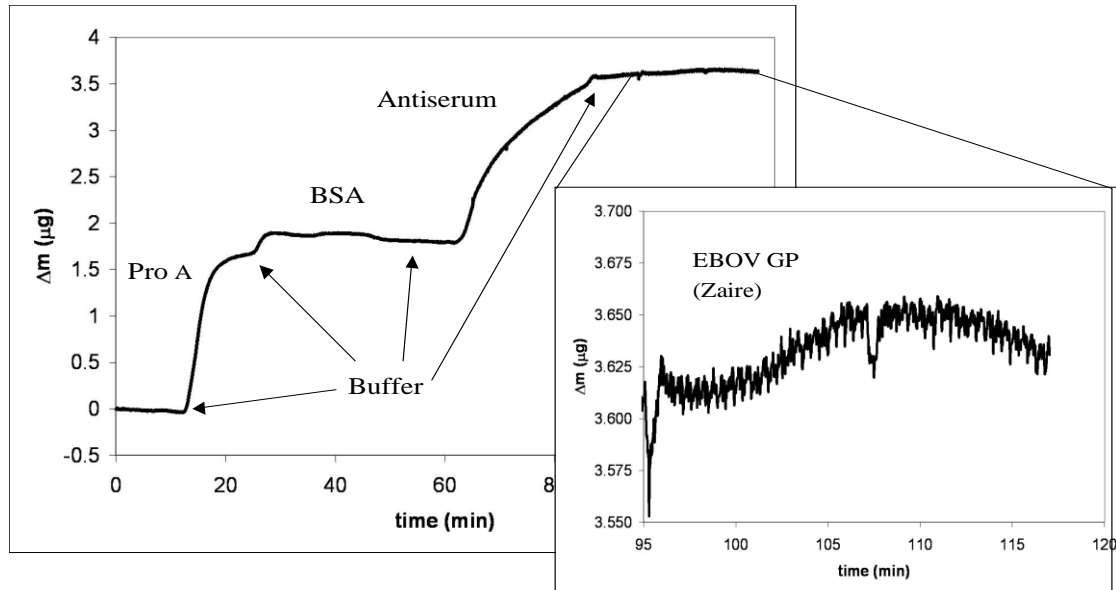


Figure 24. Plot of the polyclonal antibodies used with Protein A. Antiserum showed very large mass gains, which could be attributed to non-specific adsorption.

$1.8 \pm 0.2 \mu\text{g}$. Since this sample is from sera, it contains cells, proteins, and antibodies outside of the Ebola specific antibodies. These excess proteins could find ways to layer on the biosensor nonspecifically, either onto the gold or by aggregating on itself. This likely leads to less active antibody for binding because the Protein A will be covered with non-ebola IgG's, and extra serum proteins will layer the antibodies themselves. BSA did not bind very much for all experiments, much like the trials performed with Protein A that were previously described. Binding was seen at very high concentrations of the GP, in the range of 196 nM for both GP strains.

Table 2 summarizes the experiments performed using the monoclonal and polyclonal antibodies to detect the ebola GP. Again, the 15H10 antibody was determined to have the greatest binding out of the four tested. Both 15H10 and 6D11 show a preference for the Zaire GP over the Sudan-Gulu GP.

Antibody	Capture Agent Used	Capture Agent Δm (μg)	Antibody Δm (μg)	Zaire (nM)	Sudan-Gulu (nM)
Rabbit antiserum	Protein A	1.6 + 0.3	1.8 + 0.2	196	196
6D11	Protein G	0.9 + 0.2	0.56 + 0.09	130	160
15H10	Protein A	1.8 + 0.2	0.6 + 0.1	14	56
17A3	Protein L	0.36 + 0.04	1.3 + 0.1	-	-

Table 2. Summary table of the Ebola GP screening, showing capture agent mass binding, and antibody mass binding.

Binding efficiency is a large consideration in any biosensor that wants to achieve the best detection. QCM is very useful because the mass can be calculated at each step, which can then be transformed into the number of molecules and area coverage. The estimations show that Protein A is forming approximately 2.5 layers and Protein G is forming about 3. Then antibody coverage can be calculated bound to the capture agent from the mass graph. The data showed about 23% coverage of 15H10 on Protein A and 25% for 6D11 on Protein G. The collection efficiency of the antibody to antigen determines how well the antibody is binding glycoprotein from the bulk solution. This calculation is simply the bulk solution divided by the amount bound. The 15H10-Zaire system starts with a collection efficiency of about 2% for the lowest concentration, and decreases to about 0.6% for the highest concentration. The 15H10-Sudan-Gulu pair has a much narrower collection window, with 1.0% at the lowest concentrations and 0.8% at the highest concentrations.

Covalent Biosensor Assemblies

In order to improve upon the already developed ebola GP biosensor, efforts were made to create a more stable, reusable sensor. A series of biosensors were constructed that had covalent attachment stemming from the gold QCM electrode to the antibody.

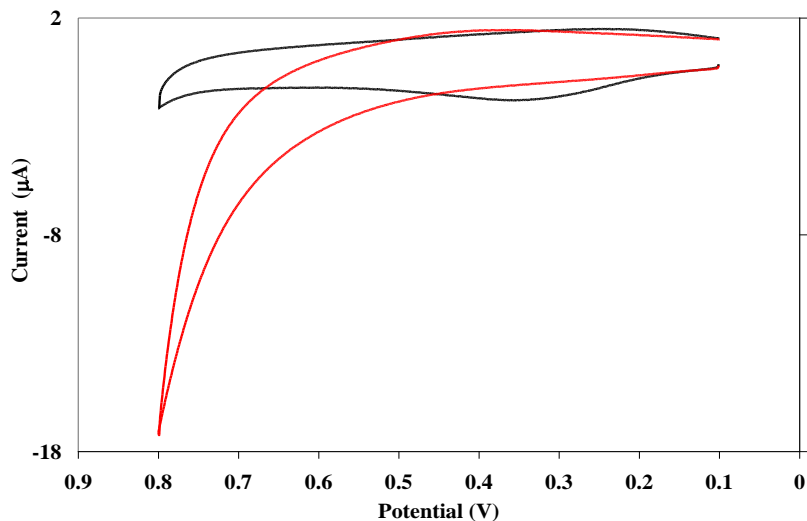


Figure 25. Cyclic voltammetry of the gold QCM electrode shows normal oxidation and reduction before the addition of a SAM (black). Post-SAM formation the oxidation/reduction no longer show (red).

The strategy here was to selectively reduce the antibody along the backbone to have a free thiol for attachment. The first layer on the QCM was the aminoethanethiol, which will form a SAM with the thiol on the gold and leave the amine group free to react. This group does not show up on mass graphs because it has a very low molecular weight, and because of this, the procedure was changed to making SAMs outside the QCM for 12 hours. The increased time let the SAM form a more stable arrangement. Cyclic voltammetry in Figure 25 shows the removal of the gold oxidation/reduction peaks after

the addition of the aminoethanethiol, showing that there is good surface coverage. As a second verification, the large current at -0.8 mV indicates the removal of the SAM. The next group used was the Sulfo-SMCC, which has a reactive maleimide group and a reactive NHS group. The NHS will form a bond with the free amine on the SAM, this leaves the maleimide group free to bond with thiols from the antibody. The selectivity of each reactive end group has been previously monitored by FT-IR.⁵⁷ If this step was done in the QCM it was run for 10 minutes, as a SAM it was allowed one hour to form.

Next, the antibody was reduced with DTT and purified in a Sephadex G-10

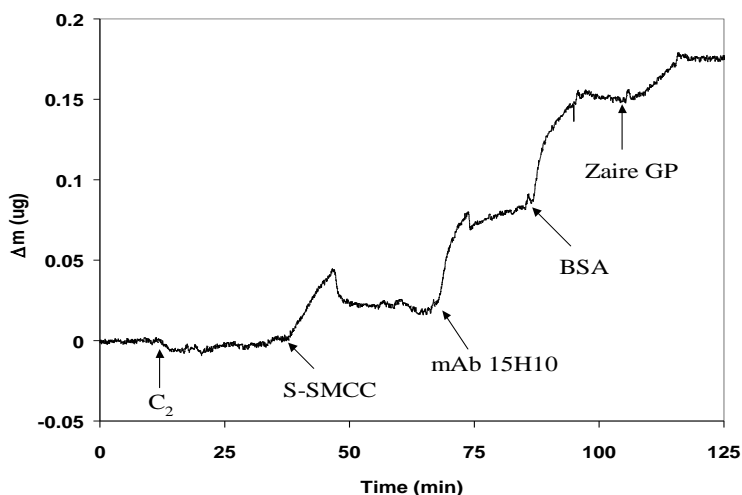


Figure 26: Gravimetry of the aminoethanethiol covalent biosensor.

column to separate DTT from antibody. Antibody was obtained and characterized via UV-VIS. Once the purified antibody was separated it was added to the QCM crystal immediately to avoid formation of the thiol bridge. In the QCM, the antibody was given 10 minutes of flow as seen in figure 26. As a SAM it was allowed one hour to react with the maleimide group. The recorded antibody gain was about $0.06 \pm 0.01 \mu\text{g}$. This is 10%

of the antibody mass that was bound for the capture assay. Zaire GP binding was observed with this technique, but to a lesser extent than with the original antibody capture assays. GP binding was shown to be $0.027 \pm 0.004 \mu\text{g}$, which is approximately half of what was observed with the first capture assays.

Capture Agent-Antibody Crosslinking

Another avenue to a reusable sensor is crosslinking the antibody to the capture agent. This strategy assures antibody orientation and retains the natural conformation. Crosslinking was done as a SAM in order to give the BS³ time to form bonds with the free amines on both the Protein A and antibody. Because we used the same combination of Protein A-15H10, the initial layer is assumed to be that of the original trials. The crystals equilibrated quickly in the QCM and were then subjected to BSA to block any remaining sites. BSA did not show much, if any, mass binding during runs. Zaire GP was run for 10 minutes at 20 $\mu\text{g/mL}$ as before, and showed repeated binding of 12 ng, Figure 27. The washing buffer was a high salt concentration PBS (50 mM PB, 1 M NaCl). The high salt will break any electrostatic interactions between the antibody and antigen at the binding site. The downside to the high concentration of salt is that it causes the measured resistance to change drastically, and recover very slowly. A low pH washing buffer may be more appropriate for the QCM because it will carry less ions to disrupt the sensor.

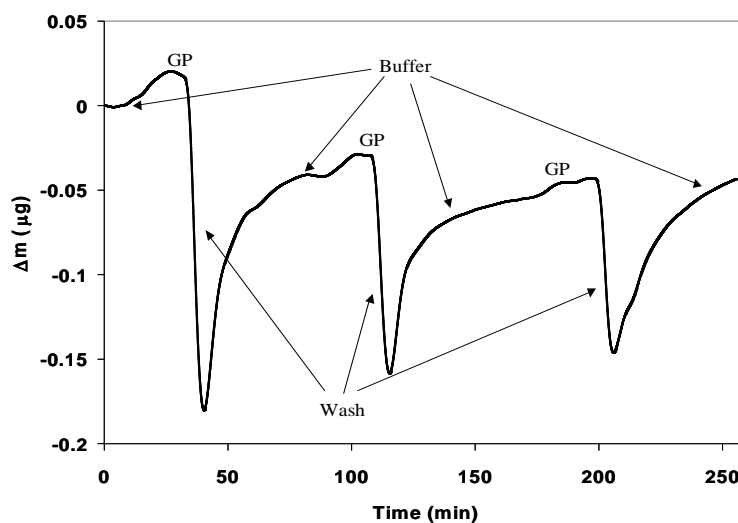


Figure 27: Glycoprotein detection on the crosslinked ProA-mAb15H10, showing 3 repeated detections. Graph is filtered at 0.1 Hz.

Attachment Methods Summary

While the two assays described above were the most successful attempts for binding the GP, a wide variety of linking methods were tested. Table 3 summarized these attempts based on how they connected the antibody to the QCM surface. The first group is the classic antibody-capture agent, where the surface is first modified with a capture protein and the antibody is recognized and bound to the surface. From here, the second column shows methods used to directly link the antibody to the gold surface using SAM chemistry. Typically, the antibody is first reduced along the labile disulfide and then added to solution to remake a sulfur bridge to the surface. Lastly, in the third class the antibodies were recognized by a capture agent to assure orientation, but then they were crosslinked to the capture agent, using either BS³ or gluteraldehyde. Accompanying graphs are shown in Appendix A.

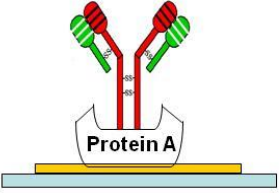
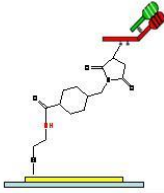
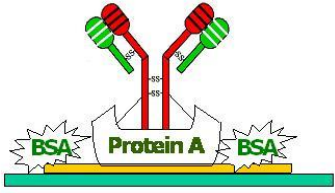
Capture Agent	Covalent attachment to Gold	Covalent-Capture Agent hybrid
Protein A – Recognize mouse IgG2a	Dithiothreitol (DTT) – Reduce IgG disulfide to make antibody SAM	BS³ – Directly tether antibody to Protein A by linking amines on both proteins
Protein G – Recognize mouse IgG1	Traut's Reagent – Convert amines to thiols to make a SAM	Gluteraldehyde – Crosslink the antibody to Protein A or other antibodies
Protein L – Binds kappa-light chain, mouse igG1 and IgM	1,6 – hexanedithiol - Make initial SAM then link antibody to SAM	
	Amide coupling – Couple IgG carboxylic acid group to amine terminated SAM	
		

Table 3. Summary of different methods used to link the antibody to the QCM surface. The cartoons show how each methods links the antibody and QCM.

Conclusions

The QCM biosensor described here has successfully detected and quantified ebolavirus glycoprotein using antibodies specific to the protein. The QCM assay is more rapid than both ELISA and RT-PCR, and measures binding on the nanogram scale. The paneling experiment used four different antibodies against two strains of ebolavirus. The K_a from the 15H10-Zaire pair was $9 \pm 1 \times 10^6 \text{ M}^{-1}$ with a detection limit of 14 nM followed closely by the 15H10-Sudan system with a detection limit of 56 nM. The K_a values for the remaining systems could not be determined because of the non-Langmuirian behavior observed. Simultaneously, the binding and collection efficiencies

were calculated at the different concentrations. Multilayer formation was observed for the Protein A and G layers, while 25% packing was measured for the antibodies. The GP had fairly low efficiencies at 2% maximum. Despite the collection efficiencies, the sensor did detect the GP in a rapid fashion, opening the door for a quick detection method for ebolavirus, using a facile methodology that can easily be translated to the field.

References

- (1) Yu, J.-S.; Liao, H.-X.; Gerdon, A. E.; B., H.; Scarce, R. M.; McAdams, M.; Alam, S. M.; Popernack, P. M.; Sullivan, N. J.; Wright, D.; Cliffel, D. E.; Nabel, G. J.; Haynes, B., B.F. *J. Virol. Methods* **2006**, *137*, 137-228.
- (2) Prevention, C. f. D. C. a. 2002; Vol. 2007.
- (3) Leeroy, E. M.; Baize, S.; Lu, C. Y.; McCormick, J. B.; Georges, A. J.; Georges-Courbot, M.-C.; Lansoud-Soukate, J.; Hoch-Fisher, S. P. *J. Med. Vir.* **2000**, *60*, 463-467.
- (4) Towner, J. S.; Rollin, P. E.; Bausch, D. G.; Sanchez, A.; Crary, S. M.; Vincent, M.; Lee, W. F.; Spiropoulou, C. F.; Ksiazek, T. G.; Lukwiya, M.; Kaducu, F.; Dowling, R.; Nichol, S. T. *J. Virol.* **2004**, *78*, 4330-4341.
- (5) Weidmann, M.; Mühlberger, E.; Hufert, F. T. *J. Clin. Vir.* **2004**, *30*, 94-99.
- (6) Sanchez, A.; Lukwiya, M.; Bausch, D.; Mahanty, S.; Sanchez, A. J.; Wagoner, K. D.; Rollin, P. E. *J. Virol.* **2004**, *78*, 10370-10377.
- (7) Ikegami, T.; Niikura, M.; Saijo, M.; Miranda, M. E.; Calaor, A. B.; Hernandez, M.; Acosta, L. P.; Manalo, D. L.; Kurane, I.; Yoshikawa, Y.; Morikawa, S. *Clin. Diagn. Lab. Immunol.* **2003**, *10*, 552-557.
- (8) Kallstrom, G.; Warfield, K. L.; Sweson, D. L.; Mort, S.; Panchal, R. G.; Ruthel, G.; Bavari, S.; Aman, M. J. *J. Virol. Methods* **2005**, *127*, 1-9.
- (9) Niikura, M.; Ikegami, T.; Saijo, M.; Kurane, I.; Miranda, M. E.; Morikawa, S. *J. Clin. Microbiol.* **2001**, *39*, 3267-3271.
- (10) Kurosaki, Y. T., A.; Ebihara, H.; Grolla, A.; Kamo, N.; Feldmann, H.; Kawaoka, Y.; Yasuda, J. *J. Virol. Methods* **2006**.
- (11) Sanchez, A.; Rollin, P. *Vir. Res.* **2005**, *113*, 16-25.
- (12) Bosio, C. M.; Moore, B. D.; Warfield, K. L.; Ruthel, G.; Mohamadzadeh, M.; Aman, M. J.; Bavari, S. *Virology* **2004**, *326*, 280-287.
- (13) Janshoff, A. G., H.-J.; Steinem, C. *Angew. Chem. Int. Ed.* **2000**, *39*, 4004-40032.
- (14) Martin, S. J.; Bandey, H. L.; Cernosek, R. W.; Hillman, A. R.; Brown, M. *J. Anal. Chem.* **2000**, *72*.
- (15) Sauerbrey, G. *Z. Phys.* **1959**, *115*, 206.
- (16) Gerdon, A. E.; Wright, D. W.; Cliffel, D. E. *Anal. Chem.* **2005**, *77*, 304-310.

- (17) Zhang, Y. T., V.; Sathe, M.; Zeng, X.; Wang, P.G. *J. Am. Chem. Soc.* **2003**, *125*, 9292-9293.
- (18) Maxtek, I., Operation and Service Manual - Research Quartz Crystal Microbalance.
- (19) Muramatsu, H. T., E.; Karube, I. *Anal. Chem.* **1988**, *60*, 2142-2146.
- (20) Ebara, Y. I., K.; Okahata, Y. *Langmuir* **1996**, *12*, 5165-5170.
- (21) Gerdon, A. E.; Wright, D. W.; Cliffler, D. E. In *Nanosystem Characterization Tools in the Life Sciences*; Kumar, C. S. S. R., Ed.; Wiley-VCH: 2006; Vol. 3, p 109-144.
- (22) Karpovic, D. S. B., G.J. *Langmuir* **1994**, *10*, 3315-3322.
- (23) Keil, R. G., Thermodynamics-Kinetics at the QCM - Notes.
- (24) Ebara, Y.; Itakura, K.; Okahata, Y. *Langmuir* **1996**, *12*, 5165-5170.
- (25) Karpovich, D. S.; Blanchard, G. J. *Langmuir* **1994**, *10*, 3315-3322.
- (26) Ebato, H.; Gentry, C. A.; Herron, J. N.; Müller, W.; Okahata, Y.; Ringsdorf, H.; Sucl, P. A. *Anal. Chem.* **1994**, *66*, 1683-1689.
- (27) Gerdon, A. E.; Wright, D. W.; Cliffler, D. E. *Biomacromolecules* **2005**, *6*, 3419-3424.
- (28) Wu, T.-Z.; Su, C.-C.; Chen, L.-K.; Yang, H.-H.; Tai, D.-F.; Peng, K.-C. *Biosesn. Bioelectron.* **2005**, *21*, 689-695.
- (29) Zuo, B.; Li, S.; Guo, Z.; Zhang, J.; Chen, C. *Anal. Chem.* **2004**, *76*, 3536-3540.
- (30) Hu, J.; Liu, L.; Danielsson, B.; Zhou, X.; Wang, L. *Anal. Chim. Acta* **2000**, *423*, 215-219.
- (31) Skládal, P.; Riccardi, C. d. S.; Yamanaka, H.; Costa, P. I. d. *J. Vir. Met.* **2004**, *117*, 145-151.
- (32) Aberl, F.; Wolf, H.; Kößlinger, C.; Drost, S.; Woias, P.; Koch, S. *Sens. Actuators, B* **1994**, *18-19*, 217-275.
- (33) König, B.; Grätzel, M. *Anal. Chem.* **1994**, *66*, 341-344.
- (34) Uttenthaler, E.; Schräml, M.; Mandel, J.; Drost, S. *Biosesn. Bioelectron.* **2001**, *16*, 735-743.
- (35) Lee, Y. G.; Chang, K. S. *Talanta* **2005**, *65*, 1335-1342.
- (36) Abad, J. M.; Pariente, F.; Hernández, L.; Lorenzo, E. *Anal. Chim. Acta* **1998**, *368*, 183-189.
- (37) Kößlinger, C.; Uttenthaler, E.; Drost, S.; Aberl, F.; Wolf, H.; Brink, G.; Stanglmaier, A.; Sackmann, E. *Sens. Actuators, B* **1995**, *24-25*, 107-112.
- (38) Smith, E. A.; Thomas, W. D.; Kiessling, L. L.; Corn, R. M. *J. Am. Chem. Soc.* **2003**, *125*, 6140-6148.
- (39) Okahata, Y.; Ebato, H. *Anal. Chem.* **1989**, *61*, 2185-2188.
- (40) Zhang, Y.; Telyatnikov, V.; Sathe, M.; Zeng, X.; Wang, P. G. *J. Am. Chem. Soc.* **2003**, *125*, 9292-9293.
- (41) Pyun, J. C.; S.D., K.; Chung, J. W. *Anal. Biochem.* **2005**, *347*, 227-233.
- (42) Wang, H.; Castner, D. G.; Ratner, B. D.; Jiang, S. *Langmuir* **2004**, *20*, 1877-1887.
- (43) Bachelder, E. M.; Ainslie, K. M.; Pishko, M. V. *Sensor Lett.* **2005**, *3*, 211-215.

- (44) Spangler, B. D.; Wilkinson, E. A.; Murphy, J. T.; Tyler, B. J. *Anal. Chim. Acta* **2001**, *444*, 149-161.
- (45) Kößlinger, C.; Drost, S.; Aberl, F.; Wolf, H.; Koch, S.; Woias, P. *Biosesn. Bioelectron.* **1992**, *7*, 397-404.
- (46) Kößlinger, C.; Drost, S.; Aberl, F.; Wolf, H. *J. Anal. Chem.* **1994**, *349*, 349-354.
- (47) Leopold, M. C.; Bowden, E. F. *Langmuir* **2002**, *18*, 2239-2245.
- (48) Patel, N.; Davies, M. C.; Hartshorne, M.; Heaton, R. J.; Roberts, C. J.; Tandler, S. J. B.; Williams, P. M. *Langmuir* **1997**, *13*, 6485-6490.
- (49) Hutter, E.; Fendler, J. H.; Roy, D. *J. Phys. Chem. B* **2001**, *105*, 11159-11168.
- (50) Björck, L. *J. Immunol.* **1988**, *140*, 1194-1197.
- (51) Briand, E.; Salmain, M.; Herry, J.-M.; Perrot, H.; Compère, C.; Pradier, C.-M. *Biosesn. Bioelectron.* **2006**, *22*, 440-448.
- (52) Schmid, A. H.; Stanca, S. E.; Thakur, M. S.; Thampi, K. R.; Suri, C. R. *Sens. Actuators, B* **2006**, *113*, 297-303.
- (53) Willis, H. E.; Browder, B.; Feister, A. J.; Mohanakumar, T.; Ruddy, S. *J. Immunol.* **1988**, *140*, 234-239.
- (54) Wang, H.; Zeng, H.; Shen, G.; Yu, R. *Anal. Chem.* **2006**, *78*, 2571-2578.
- (55) PierceBiotechnologies **2003**.
- (56) Caruso, F.; Rodda, E.; Furlong, D. N. *J. Colloid Interface Sci.* **1996**, *178*, 104-115.
- (57) Frey, B. L.; Corn, R. M. *Anal. Chem.* **1996**, *68*, 3187-3193.